

## Au nano dendrites/composition optimized Nd-doped cobalt oxide as an efficient electrocatalyst for ethanol oxidation

Foroozan Hasanpour<sup>a,\*</sup>, Masoumeh Taei<sup>a</sup>, Masoud Fouladgar<sup>b</sup>, Mehdi Salehi<sup>c</sup>

<sup>a</sup>Department of Chemistry, Payame Noor University, 19395-4697 Tehran, Iran

<sup>b</sup>Department of Biochemistry, Falavarjan Branch, Islamic Azad University, Isfahan, Iran

<sup>c</sup>Department of Chemistry, Semnan University, Semnan 35351-19111, Iran

Received: 24 August 2019, Accepted: 20 March 2020, Published: 01 April 2020

### Abstract

In this study, Nd-doped cobalt oxide (Nd-Co<sub>3</sub>O<sub>4</sub>) nanoparticles were prepared by a combustion synthesis procedure using Co(acac)<sub>3</sub> complex. The nanoparticles were characterized by infrared spectroscopy (IR), X-ray diffraction (XRD), scanning electron microscopy (SEM) and energy-dispersive X-ray spectroscopy (EDX). Then, the effect of Nd-Co<sub>3</sub>O<sub>4</sub> on the electrocatalytic activity of gold nanodendrites (AuNDs) electrodeposited on a glassy carbon electrode (GCE) for ethanol oxidation was studied. The results showed that the Nd-Co<sub>3</sub>O<sub>4</sub>/AuNDs/GCE presents higher active surface area and current density (about 2 times) for the ethanol oxidation compared with the AuNDs/GCE. Cyclic voltammetry and chrono-potentiometry methods proved that the Nd-Co<sub>3</sub>O<sub>4</sub>/AuNDs/GCE is able to increase a long-term stability of electrode in alkaline ethanol fuel cell by providing OH<sub>ads</sub> species at the surface of the catalysts. Consequently, the Nd-Co<sub>3</sub>O<sub>4</sub>/AuNDs/GCE, as an anodic electrode, reveals potent catalytic activity for ethanol oxidation in alkaline media.

**Keywords:** Nd-doped cobalt oxide nanoparticles; ethanol oxidation; alkaline fuel cells; Au nano dendrites.

### Introduction

In recent years, a significant effort has been made to improve the electrocatalytic oxidation of alcohols because of their potentials as liquid fuel with a high energy density in fuel cells [1,2]. The electrocatalyst material should have characteristics such as low onset potential, low over potential and larger current density for fuel oxidation. Cobalt based metal oxides are getting more attention for electrooxidation of C<sub>1</sub>, C<sub>2</sub> and C<sub>3</sub> alcohols due to the

improvement of the oxidation kinetics of these alcohol in alkaline media [3,4]. Cubic Co<sub>3</sub>O<sub>4</sub> has spinel structure consisting of one Co<sup>2+</sup> in the tetrahedral site and two Co<sup>3+</sup> in octahedral site. Replacement of cobalt ions in a cobalt oxide spinel structure by other metals can tune its electrocatalytic activity [5,6]. It has been proven that Lanthanides-based nanomaterials can be used as catalysts and/or co-catalysts in different types of fuel cells [7,8]. It is expected that Lanthanide-doped Co<sub>3</sub>O<sub>4</sub>

upgrades catalytic activity toward ethanol oxidation than  $\text{Co}_3\text{O}_4$  alone. Noble nano-sized particles such as Au and Pt are generally accepted as excellent electrocatalysts for  $\text{C}_1$  and  $\text{C}_2$  alcohol oxidation [9,10]. However, slow kinetics and easy poisoning have reduced the application of Pt and Pt-based catalysts in fuel cells. Unlike Pt, Au doesn't undergo serious poisoning by chemisorbed carbonaceous intermediates during the oxidation of alcohols [11,12]. Some problems such as their high cost and limited supply can be resolved by the combination of noble metals with low cost active metals or oxides. In the present work, the effect of cobalt oxide-doped neodymium oxide ( $\text{Co}_{3-x}\text{Nd}_x\text{O}_4$ ) on the catalytic activity of Au was studied.  $\text{Co}_{3-x}\text{Nd}_x\text{O}_4$  was synthesized from  $\text{Co}(\text{acac})_3$  complex by combustion method. Then it was applied for coating electrodeposited AuNDs on a GCE. The electrocatalytic activity of the Nd- $\text{Co}_3\text{O}_4/\text{AuNDs}/\text{GCE}$  for ethanol oxidation was compared with the  $\text{AuNDs}/\text{GCE}$  and  $\text{AuNDs}/\text{Nd-Co}_3\text{O}_4/\text{GCE}$  using cyclic voltammetry and chrono-potentiometry methods. The results showed that the ethanol oxidation in alkaline media at Nd- $\text{Co}_3\text{O}_4/\text{AuNDs}/\text{GCE}$  takes place with a higher current density compared to the  $\text{AuNDs}/\text{GCE}$ .

## **Experimental**

### *Instrumentations and chemicals*

All chemicals were of analytical grades and purchased from Sigma-Aldrich. The structure and morphology of nanoparticles were studied using X-ray diffraction (XRD, Holland Philips Xpert diffractometer with  $\text{Cu-K}\alpha$  radiation) and field emission scanning electron spectroscopy (FE-SEM, Hitachi S-4160, Japan), respectively. FT-IR spectra were recorded using JASCO FTIR-4100 spectrometer. All

electrochemical experiments were performed using an Autolab potentiostat/galvanostat (Model PGSTAT302) or Metrohm instrument (Model 797 VA). The electrochemical instrument was equipped with a three-electrode cell containing a platinum counter electrode,  $\text{Ag}/\text{AgCl}$  as a reference electrode and a modified/unmodified glassy carbon electrode (GCE) as a working electrode.

### *Synthesis of $\text{Co}_{3-x}\text{Nd}_x\text{O}_4$ nanoparticles*

$\text{Co}(\text{acac})_3$  complex was needed as a precursor for synthesis of  $\text{Co}_{3-x}\text{Nd}_x\text{O}_4$  nanoparticles. Therefore, it was made by dissolving 0.38 g of cobalt (II) acetate into 5.0 mL hot distilled water (at temperature of 90 °C). Then, 5.0 mL acetylacetone and 4.5 mL hydrogen peroxide solution (10% v/v) were added to the above solution while stirring. After 15 minutes, the mixture was cooled in ice water bath for 30 minutes. The solution color changed to dark green. Afterwards, it was filtered under vacuum. The crystalline product was dried in an oven at 100 °C. Appropriate molar amounts of synthesized  $\text{Co}(\text{acac})_3$  and  $\text{Nd}_2\text{O}_3$  were mixed into a crucible and warmed in a furnace at 700 °C for 8 h. Nanoparticles of  $\text{Co}_{3-x}\text{Nd}_x\text{O}_4$  ( $x=0.01, 0.03$  and  $0.05$ ) were synthesized under these conditions [13,14].

### *Electrode preparation*

A bare GCE was polished with 5  $\mu\text{m}$  alumina slurry, and then sonicated in a mixture of ethanol/distilled water solution (50% v/v) for 10 min. Au electrodeposition on the GCE was carried out by applying a constant potential of  $-0.20$  V during 210 s in an aqueous solution of  $4.0 \times 10^{-3}$  mol  $\text{L}^{-1}$   $\text{HAuCl}_4 \cdot 3\text{H}_2\text{O}$  and  $0.10$  mol  $\text{L}^{-1}$   $\text{KNO}_3$ . Then, the synthesized Nd- $\text{Co}_3\text{O}_4$  powder was dispersed in distilled

water (0.10 mg per 10 mL) using ultrasonic agitation and allowed to obtain homogeneous suspension. Finally, 5.0  $\mu\text{L}$  of the suspension was dropped on the GCE until dried at room temperature.

### Results and discussion

#### *Characterizations of the synthesized Nd-Co<sub>3</sub>O<sub>4</sub> powder and Co<sub>3-x</sub>Nd<sub>x</sub>O<sub>4</sub>/AuNDs/GCE*

Figure 1A shows the XRD patterns of spinel cubic structure of Co<sub>3</sub>O<sub>4</sub> (curve a). Diffraction lines were detected at  $2\theta=19.0^\circ$ ,  $31.2^\circ$ ,  $36.5^\circ$ ,  $38.4^\circ$ ,  $44.8^\circ$ ,  $55.6^\circ$ ,  $59.0^\circ$  and  $65.2^\circ$ , which corresponding to the reflections of (1 1 1), (2 0 0), (3 1 1), (2 2 2), (4 0 0), (4 2 2), (5 1 1) and (4 4 0), respectively [15]. With the increasing of the Nd<sup>3+</sup> amount from  $x = 0.01$  (curve b) to 0.03 (curve c), no additional XRD line pertaining to any secondary phase was observed. Therefore, it is concluded that Co<sup>3+</sup> is replaced with Nd<sup>3+</sup>. Further addition of Nd<sup>3+</sup> ( $x=0.05$ ) leads to emergence of an additional peak at  $2\theta = 61.8^\circ$ , which confirms that the excess of the Nd<sup>3+</sup> ions resided on the surface or on the grain boundaries of the Co<sub>3-x</sub>Nd<sub>x</sub>O<sub>4</sub> (curve d) [16,13,14]. Thus, the maximum amount of Nd-doped is selected to be 0.03. FT-IR spectra of

Co<sub>3</sub>O<sub>4</sub> and Co<sub>3-x</sub>Nd<sub>x</sub>O<sub>4</sub> nanoparticles are shown in Figure 1B. FT-IR of Co<sub>3</sub>O<sub>4</sub> (curve e) displays two distinct bands at 576 ( $\nu_1$ ) and 665 ( $\nu_2$ )  $\text{cm}^{-1}$  which originate from the stretching vibrations of the Co-O bonds, demonstrating the formation of Co<sub>3</sub>O<sub>4</sub> spinel oxide [17]. The  $\nu_1$  band is characteristic of Co<sup>3+</sup> vibration in the octahedral hole, and  $\nu_2$  band is attributed to Co<sup>2+</sup> vibration in tetrahedral hole in the spinel lattice [18]. Two peak absorptions at the wavenumber range of 1200-1700  $\text{cm}^{-1}$  (curve f) confirm the presence of Nd oxide inside Co<sub>3</sub>O<sub>4</sub> spinel and the ability of the Nd oxide to form weak surface carbonates upon exposure to the atmospheric air. The SEM image of Co<sub>3</sub>O<sub>4</sub> spinel (Figure 2A) shows the non-spherical shape of micro-particles with a number of holes on their surface. Figure 2 (B, C and D) shows the SEM images of the Co<sub>3</sub>O<sub>4</sub> after Nd<sup>3+</sup> doping (i.e. Co<sub>3-x</sub>Nd<sub>x</sub>O<sub>4</sub>) when  $x = 0.01$ , 0.03 and 0.05 molar ratio, respectively. According to these images, the nanoparticles have average particle size about 40-50 nm. It is obvious that the morphology of Co<sub>3-x</sub>Nd<sub>x</sub>O<sub>4</sub> is more uniform compared to un-doped spinel.

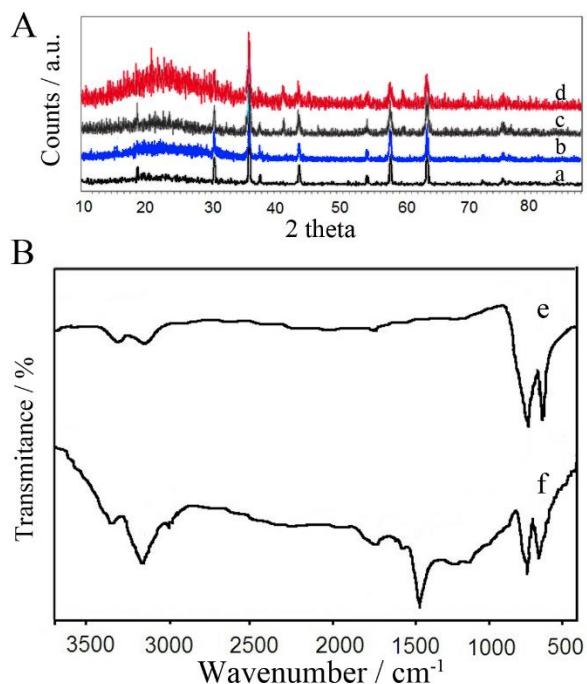


**Figure 1.** (A) The XRD pattern of (a) Co<sub>3</sub>O<sub>4</sub>, (b) Co<sub>3-x</sub>Nd<sub>x</sub>O<sub>4</sub> (X=0.01), (c) Co<sub>3-x</sub>Nd<sub>x</sub>O<sub>4</sub> (X=0.03), (d) Co<sub>3-x</sub>Nd<sub>x</sub>O<sub>4</sub> (X=0.05), (B) FT-IR spectra of undoped (e) Co<sub>3</sub>O<sub>4</sub> and (f) Nd-doped Co<sub>3</sub>O<sub>4</sub> nanocrystals.

The FE-SEM images of AuNDs electrodeposited at GCE and Nd<sub>0.03</sub>Co<sub>2.97</sub>O<sub>4</sub> coated on AuNDs/GCE have been displayed in Figure 3A and B, respectively. As can be seen clearly in curve A, after Au electrodeposition, both nano spherical and micro/nano dendritic gold structures are deposited

at the surface of the GCE. By increasing the electrodeposition time, they start to grow in different directions and finally form micro/nano dendrites. FE-SEM image of Nd<sub>0.03</sub>Co<sub>2.97</sub>O<sub>4</sub> coated on AuNDs/GCE surface is shown in Figure 3B.

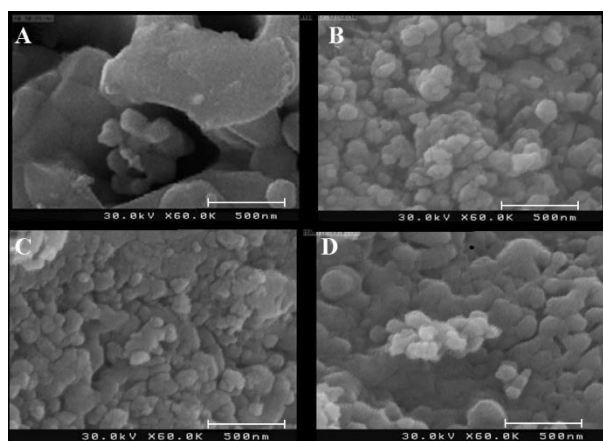


**Figure 2.** SEM images of (A) undoped Co<sub>3</sub>O<sub>4</sub>, and Co<sub>3-x</sub>Nd<sub>x</sub>O<sub>4</sub> with x equal to (B) 0.01, (C) 0.03, and (D) 0.05.

From the close inspection, it is found that the wide surface of AuNDs is covered by Nd<sub>0.03</sub>Co<sub>2.97</sub>O<sub>4</sub> particles. EDX analysis shows the elemental

composition of the catalyst, which confirms the presence of both of the Nd<sub>0.03</sub>Co<sub>2.97</sub>O<sub>4</sub> and AuNDs at the surface of the GCE (Figure 3C).

Transmission electron microscopic (TEM) image of synthesized  $\text{Co}_3\text{O}_4$  confirms formation of spindle-like morphology and multigonal particles (Figure 4 A). The particles have been distributed uniformly in the powder sample. In addition, TEM image of  $\text{Nd}_{0.03}\text{Co}_{2.97}\text{O}_4$  shows that nanoparticles have been synthesized uniformly and agglomeration of particles has not been occurred (Figure 4B).

#### Ethanol electrooxidation

Figure 5A displays cyclic voltammograms of GCE (a), AuNDs/ $\text{Nd}_{0.03}\text{Co}_{2.97}\text{O}_4$ /GCE (b), AuNDs/GCE (c),  $\text{Nd}_{0.03}\text{Co}_{2.97}\text{O}_4$ /GCE (d) and  $\text{Nd}_{0.03}\text{Co}_{2.97}\text{O}_4$ /AuNDs/GCE in a solution of  $0.5 \text{ mol L}^{-1}\text{KOH}$  with a scan rate of  $50 \text{ mV s}^{-1}$ . At the GCE, no redox peak is seen in the potential range of  $-0.40$  to  $0.70 \text{ V}$  (curve a). The background current is increased by

coating the GCE with  $\text{Nd}_{0.03}\text{Co}_{2.97}\text{O}_4$ , while no redox peak is observed. After the electrodeposition of AuNDs on the GCE, a couple anodic peak at the potentials of  $0.22$  and  $0.40 \text{ V}$  and a couple cathodic peak at about  $-0.16$  and  $0.04 \text{ V}$  appear, which can be assigned to the oxidation and reduction of AuNDs, respectively [19]. Coating of  $\text{Nd}_{0.03}\text{Co}_{2.97}\text{O}_4$  on the AuNDs/GCE causes an enhancement in the current of the aforementioned cathodic and anodic peaks. In order to investigate the electrocatalytic activity of modified electrodes toward ethanol oxidation, cyclic voltammograms of these electrodes were recorded in  $0.5 \text{ mol L}^{-1}\text{KOH} + 0.50 \text{ mol L}^{-1}$  ethanol (Figure 5B). No oxidation peak appears in the presence of alkaline ethanol at the GCE and  $\text{Nd}_{0.03}\text{Co}_{2.97}\text{O}_4$ /GCE (Figure 5B curve a and e).

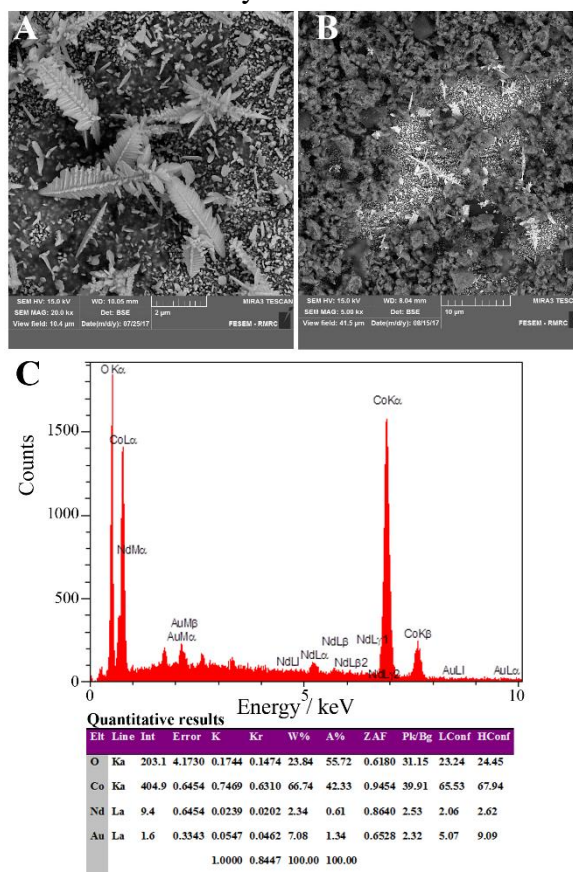
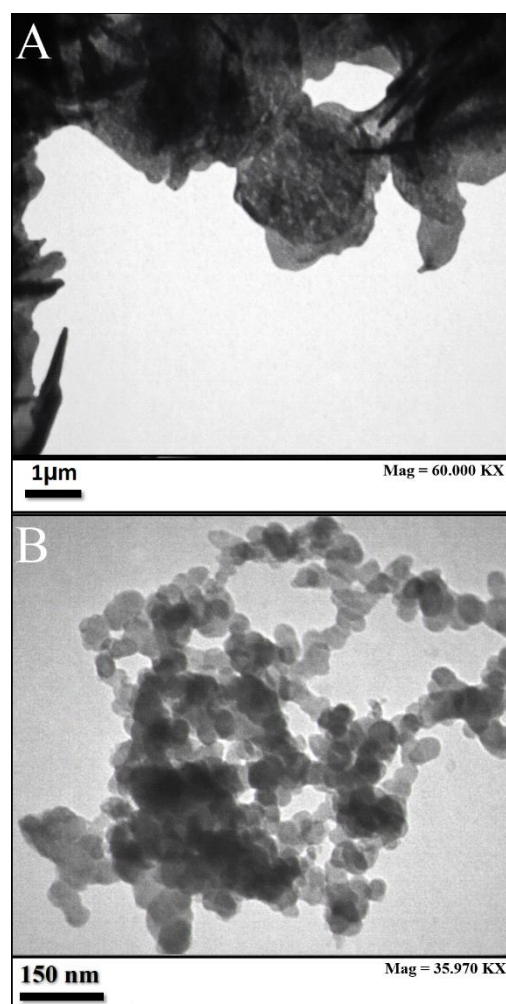
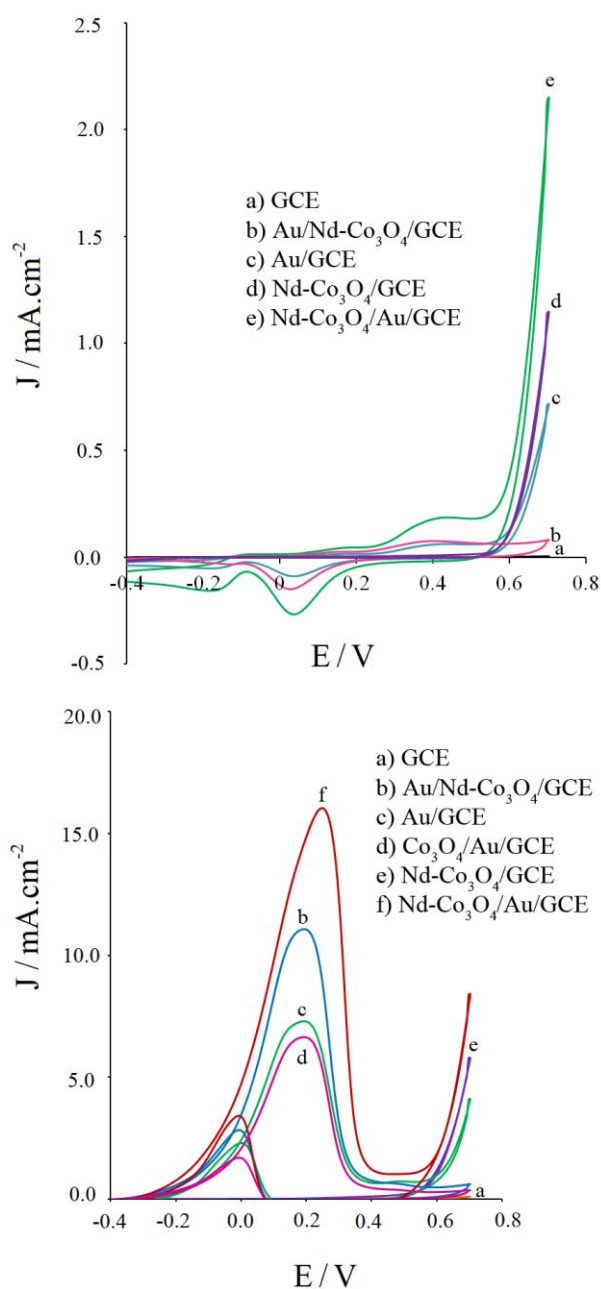


Figure 3. SEM images of (A) AuNDs/GCE, and (B)  $\text{Co}_{3-x}\text{Nd}_x\text{O}_4$  /AuNDs/GCE and (C) EDX analysis from the surface shown in B.

However, for AuNDs/GCE (Figure 5B curve c), the ethanol oxidation begins at the potential of  $-0.40$  V and continues up  $+0.40$  V. At the AuNDs/ $\text{Nd}_{0.03}\text{Co}_{2.97}\text{O}_4$ /GCE and  $\text{Nd}_{0.03}\text{Co}_{2.97}\text{O}_4$ /AuNDs/GCE (Figure 5B curve b and f, respectively), the ethanol oxidation occurs at the same potential range accompanied by higher current density. For the  $\text{Nd}_{0.03}\text{Co}_{2.97}\text{O}_4$ /AuNDs/GCE, a remarkable amplification is seen for electro-oxidation ethanol in cyclic voltammetry in comparison with the AuNDs/GCE. Three important electrocatalytic parameters including peak potential ( $E_p$ ), current density ( $J$ ) and the onset potential ( $E_{\text{onset}}$ ) for the AuNDs/GCE and  $\text{Nd}_{0.03}\text{Co}_{2.97}\text{O}_4$ /AuNDs/GCE were compared. The results show that  $J$  value at the  $\text{Nd}_{0.03}\text{Co}_{2.97}\text{O}_4$ /AuNDs/GCE surface is about 2.4 times greater than that for the AuNDs/GCE, while  $E_{\text{onset}}$  emerged at  $-0.40$  V for both of the  $\text{Nd}_{0.03}\text{Co}_{2.97}\text{O}_4$ /AuNDs and AuNDs catalysts. On the other hand,  $E_p$  for the  $\text{Nd}_{0.03}\text{Co}_{2.97}\text{O}_4$ /AuNDs occurs at more positive potentials than AuNDs.



**Figure 4.** TEM image of A)  $\text{Co}_3\text{O}_4$ , B)  $\text{Nd}_{0.03}\text{Co}_{2.97}\text{O}_4$



**Figure 5.** Cyclic voltammograms of different electrodes in (A) 0.50 mol L<sup>-1</sup>KOH; and (B) 0.50 mol L<sup>-1</sup>KOH + 0.50 mol L<sup>-1</sup>ethanol at a scan rate of 50 mV s<sup>-1</sup>.

In the case of AuNDs/Nd<sub>0.03</sub>Co<sub>2.97</sub>O<sub>4</sub>/GCE, current density is more than that of the AuNDs/GCE, but lower than the Nd<sub>0.03</sub>Co<sub>2.97</sub>O<sub>4</sub> /AuNDs/GCE. The results of cyclic voltammograms (Figure 5 B, curve a to f) indicate that

the Nd<sub>0.03</sub>Co<sub>2.97</sub>O<sub>4</sub> /AuNDs/GCE has the highest electrocatalytic activity for ethanol oxidation. As a result, Nd<sub>0.03</sub>Co<sub>2.97</sub>O<sub>4</sub> has an increasing effect on the catalytic activity of Au, especially when it is deposited on the AuNDs. In addition, it can be clearly seen that the ethanol oxidation current decreases at the AuNDs/GCE coated by Co<sub>3</sub>O<sub>4</sub>. It indicates that doping Nd into Co<sub>3</sub>O<sub>4</sub> plays a critical role in enhancing of the catalytic activity of AuNDs. As it was seen from the SEM images in Figure 2A, Co<sub>3</sub>O<sub>4</sub> has a nearly compact micro structure containing holes within, that can cover many active sites of AuNDs, and thereby prevents from the ethanol oxidation. However, Nd<sub>0.03</sub>Co<sub>2.97</sub>O<sub>4</sub> is as nanoparticles that can't cover completely the AuNDs branches. Therefore, AuNDs active sites are accessible to expose to the electrolyte, and hence the ethanol oxidation.

The effect of scan rate ( $v$ ) of CV on the ethanol oxidation was studied in the range of 10-180 mV s<sup>-1</sup>. The plot of oxidation peak current vs.  $v^{1/2}$  at both of the Co<sub>3-x</sub>Nd<sub>x</sub>O<sub>4</sub>/AuNDs/GCE and AuNDs/GCE suggests a diffusion-driven mechanism of ethanol oxidation at the surface of these electrodes.

The real active surface area ( $S_{\text{real}}$ ) of the AuNDs/GCE and Nd<sub>0.03</sub>Co<sub>2.97</sub>O<sub>4</sub>/AuNDs/GCE was calculated using Randles-Sevick formula [20] and 1mmol L<sup>-1</sup> K<sub>3</sub>Fe(CN)<sub>6</sub> as a probe in the 0.1 molL<sup>-1</sup>KCl electrolyte. From the slope of the  $I_{\text{pa}}-v^{1/2}$  relation, the active surface area was calculated as 0.064cm<sup>2</sup> for the AuNDs/GCE, 0.070 cm<sup>2</sup> for the Nd<sub>0.03</sub>Co<sub>2.97</sub>O<sub>4</sub>/AuNDs/GCE and 0.032 cm<sup>2</sup> for the GCE. The results indicate that the AuNDs structure can cause about 2-fold increases in the accessible active surface area of the electrode compared with the bare GCE. The

results also point out that  $\text{Nd}_{0.03}\text{Co}_{2.97}\text{O}_4/\text{AuNDs}$  has a bit higher active surface area than the AuNDs. As it is shown in the SEM images of the  $\text{Nd}_{0.03}\text{Co}_{2.97}\text{O}_4/\text{AuNDs}/\text{GCE}$  in Figure 3b, although the  $\text{Nd}_{0.03}\text{Co}_{2.97}\text{O}_4$  film cover the major parts of the AuNDs sites, some AuNDs branches remain out of the  $\text{Nd}_{0.03}\text{Co}_{2.97}\text{O}_4$  film. Moreover, there are many holes and pores between the  $\text{Nd}_{0.03}\text{Co}_{2.97}\text{O}_4$  nanoparticles that provides paths for electrolyte

accessibility to the AuNDs active sites. The normalized current densities (IN) were obtained as 4.2 and 8.5  $\text{mA cm}^{-2}$  for AuNDs and  $\text{Nd}_{0.03}\text{Co}_{2.97}\text{O}_4/\text{AuNDs}$ , respectively. The substantial clarification for the catalytic behavior of  $\text{Nd}_{0.03}\text{Co}_{2.97}\text{O}_4/\text{AuNDs}$  can be the presence of  $\text{OH}_{\text{ads}}$  species at the surface of the  $\text{Nd}_{0.03}\text{Co}_{2.97}\text{O}_4$ , which are used as sources of CO oxidation at the surface of electrode, and thereby the ethanol oxidation can be catalyzed.

**Table 1.** Comparison of some characteristics of the different modified electrodes oxidation of ethanol

Electrocatalyst	Preparation method	Reference electrode	Oxidation potential (mV)	Oxidation current density	Tested solution	Ref.
$\text{Cu@Pt}/\text{C}$	Core-shell structured	Hg/HgO	906	32.42 $\text{mA mg}^{-1}$	0.5 M ethanol +0.5 M NaOH	[21]
Palladium-silver polyaniline composite on GCE	Electrodeposition mode	Ag/AgCl	0	2650 ( $\text{mA. mgPd}^{-1} \cdot \text{cm}^{-2}$ )	1 M ethanol+ 0.5 M NaOH	[22]
copper oxide particles/polypyrrole on CPE	Electrodeposition	Ag/AgCl	800	2.25 $\text{mA cm}^{-2}$	0.2 M ethanol +0.1 M NaOH	[23]
Au/ Polyaniline on gold disc	Electrodeposition	SCE	310	3.36 $\text{mA cm}^{-2}$	1.0 M Ethanol +0.5 M NaOH	[24]
Au nanoflowers on carbon fiber cloth	electrodeposition	SCE	200	11.5 $\text{mA cm}^{-2}$	1.0 M ethanol+ 0.5 M NaOH	[25]
Au/ Poly(3,4-ethylenedioxythiophene) on carbon cloth	Loading onto CC sheets	SCE	157	50 $\text{mA cm}^{-2}$	1.0 M ethanol+1.0 M KOH	[26]
$\text{Nd}_{0.03}\text{Co}_{2.97}\text{O}_4/\text{AuNDs}$	Electrodeposition	Ag/AgCl	250	20.0 $\text{mA cm}^{-2}$	0.50 M KOH + 0.50 M ethanol	This work

In Table 1, the characteristics of  $\text{Nd}_{0.03}\text{Co}_{2.97}\text{O}_4/\text{AuNDs}/\text{GCE}$  were compared with some reported electrocatalysts for oxidation of ethanol. These results confirm that the proposed electrode has acceptable oxidation current and oxidation potential.

#### Catalyst stability

The intermediate species formed during ethanol oxidation can poison the active

sites of the electrode and lead to a decrease in the ethanol oxidation current. The catalyst stability was studied using CV (and chronopotentiometric methods. Cyclic voltammograms were recorded in 250 successive scans at the  $\text{Nd}_{0.03}\text{Co}_{2.97}\text{O}_4/\text{AuNDs}/\text{GCE}$  and AuNDs/GCE in 0.50mol  $\text{L}^{-1}$  KOH and 0.50 mol  $\text{L}^{-1}$  ethanol solution. There are small drifts in the anodic peaks of

ethanol during 250 cycles for the Nd<sub>0.03</sub>Co<sub>2.97</sub>O<sub>4</sub>/AuNDs/GCE while anodic current has a sharp decay after 90<sup>th</sup> cycle for the AuNDs/GCE. The results demonstrate that the intermediates at the Nd<sub>0.03</sub>Co<sub>2.97</sub>O<sub>4</sub>/AuNDs/GCE have less poisoning effects than at the AuNDs/GCE.

### Conclusion

Nd-doped cobalt oxide supported on AuNDs/GCE was fabricated. The results showed that Nd-Co<sub>3</sub>O<sub>4</sub> can upgrade the catalytic activity of AuNDs toward ethanol oxidation compared with AuNDs and Nd<sub>0.03</sub>Co<sub>2.97</sub>O<sub>4</sub> nanoparticles alone. The electrochemical measurements in alkaline media at Nd<sub>0.03</sub>Co<sub>2.97</sub>O<sub>4</sub>/AuNDs/GCE demonstrated that Nd<sub>0.03</sub>Co<sub>2.97</sub>O<sub>4</sub> containing OH<sub>ads</sub> group on the surface of AuNDs helps to catalyze the ethanol oxidation. Furthermore, the addition of Nd-Co<sub>3</sub>O<sub>4</sub> increases the resistance of AuNDs to poisoning effects of intermediates and accordingly improves its stability. Therefore, Nd-Co<sub>3</sub>O<sub>4</sub>/AuNDs/GCE represents efficient anode material for the electro catalytic oxidation of ethanol in alkaline fuel cells.

### Acknowledgements

The authors gratefully acknowledge support of this work by the Research Councils of Payame Noor University and Islamic Azad University, Falavarjan Branch.

### References

[1] P. Baile, E. Fernández, L. Vidal, A. Canals, *Analyst.*, **2019**, *144*, 366-387.  
[2] S. Sun, L. Sun, S. Xi, Y. Du, M.U. Anu Prathap, Z. Wang, Q. Zhang, A. Fisher, Z.J. Xu, *Electrochim. Acta.*, **2017**, *228*, 183-194.

[3] C. Coutanceau, S. Baranton, R.S. Bitty Kouamé, *Front. Chem.*, **2019**, *7*, 1-15.  
[4] K.K. Tintula, S. Pitchumani, P. Sridhar, A.K. Shukla, *J. Chem. Sci.*, **2010**, *122*, 381-389.  
[5] S. Sun, Z.J. Xu, *Electrochim. Acta.*, **2015**, *165*, 56-66.  
[6] S. Sun, Y. Zhou, B. Hu, Q. Zhang, Z.J. Xu, *J. Electrochem. Soc.*, **2015**, *163*, H99-H104.  
[7] E. Antolini, J. Perez, *Int. J. Hydrog. Energy*, **2011**, *36*, 15752-15765.  
[8] S.W. Song, W.S. Choi, H. Kang, S.W. Baek, A.K. Azad, J.Y. Park, J.H. Kim, *Int. J. Hydrog. Energy*, **2018**, *43*, 11378-11385.  
[9] E. Lee, I.S. Park, A. Manthiram, *J. Phys. Chem. C*, **2010**, *114*, 10634-10640.  
[10] M. Beltrán-Gastélum, M.I. Salazar-Gastélum, J.R. Flores-Hernández, G.G. Botte, S. Pérez-Sicairos, T. Romero-Castañón, E. Reynoso-Soto, R.M.R.M. Félix-Navarro, *Energy*, **2019**, *181*, 1225-1234.  
[11] G. Karim-Nezhad, S. Pashazadeh, A. Pashazadeh, *Chin. J. Catal.*, **2012**, *33*, 1809-1816.  
[12] K. Nguyen, N. Duc Hoa, C. Manh Hung, D.T. Thanh Le, N.V. Duy, N. Van Hieu, *RSC Adv.*, **2018**, *8*, 19449-19455.  
[13] M. Salehia, R. Abdoos, B. Bahramian, *J. Appli. Chem.*, **2018**, *12*, 99-116.  
[14] M. Galini, M. Salehi, M. Behza, *J. Nanostruct.*, **2018**, *8*, 391-403.  
[15] A.B. Vennela, D. Mangalaraj, N. Muthukumarasamy, S. Agilan, K.V. Hemalatha, *Int. J. Electrochem. Sci.*, **2019**, *14*, 3535-3552.  
[16] Z. Wen, L. Zhu, W. Mei, L. Hu, Y. Li, L. Sun L, *Sens. Actuators B*, **2013**, *186*, 172-179.  
[17] J.A. Gaddsdén, *Infrared Spectra of Minerals and Related Inorganic*

- Compounds, Butterworth, London, **1975**, p. 44.
- [18] H.Y. Wang, S.F. Hung, H.Y. Chen, T.S. Chan, H.M. Chen, B. Liu, *J. Am. Chem. Soc.*, **2016**, *138*, 36-39.
- [19] A.M. Ouf, A.M. Abd Elhafeez, A.A. El-Shafei, *J. Solid State Electrochem.*, **2008**, *12*, 601-607.
- [20] M. Pacios, M. Del Valle, J. Bartroli, M. Esplandiu, *J. Electroanal. Chem.*, **2008**, *619*, 117-124.
- [21] K.M. El-Khatiba, R.M. Abdel Hameed, R.S. Amin, A.E. Fetohi, *Int. J. Hydrogen Energ.*, **2017**, *42*, 14680-14696.
- [22] Z. Nodehi, A.A. Rafati, A. Ghaffarinejad, *Appl. Catal. A*, **2018**, *554*, 24-34.
- [23] A.E. Attar, L. Oularbi, S. Chemchoub, M. E. Rhazi, *Int. J. Hydrogen Energ.*, **2020**, DOI: 10.1016/j.ijhydene.2020.01.008
- [24] R.K. Pandey, V. Lakshminarayanan, *Appl. Catal. B*, **2012**, *125*, 271-281.
- [25] F. Yang, K. Cheng, K. Ye, X. Xiao, F. Guo, J. Yin, G. Wang, D. Cao, *Electrochim. Acta.*, **2013**, *114*, 478-483.
- [26] C. Wang, K. Zhang, H. Xu, Y. Du, M. C. Goh, *J. Colloid Interf. Sci.*, **2019**, *541*, 258-268.

**How to cite this manuscript:** Foroozan Hasanpour, Masoumeh Taei, Masoud Fouladgar, Mehdi Salehi. Au nano dendrites/composition optimized Nd-doped cobalt oxide as an efficient electrocatalyst for ethanol oxidation. *Iranian Chemical Communication*, 2020, 8(1), 102-111.